AGU100 ADVANCING EARTH AND SPACE SCIENCE

Journal of Advances in Modeling Earth Systems

RESEARCH ARTICLE
10.1029/2018MS001313

Energetic Constraints on the ITCZ Position in Idealized Simulations With a Seasonal Cycle

Ho-Hsuan Wei[1] **and Simona Bordoni**[1]

[1] Division of Geological and Planetary Sciences, California Institute of Technology, Pasadena, CA, USA

Key Points:
- The location of the zero total energy transport (EFE) is a good ITCZ predictor on seasonal and longer time scales
- On subseasonal time scales, the EFE leads the ITCZ and the two do not always reside in the same hemisphere
- The gross moist stability of the Hadley circulation cannot be assumed as constant and can in fact become negative during the seasonal cycle

Correspondence to:
H.-H. Wei,
hwei@caltech.edu

Citation:
Wei, H.-H., & Bordoni, S. (2018). Energetic constraints on the ITCZ position in idealized simulations with a seasonal cycle. *Journal of Advances in Modeling Earth Systems*, *10*, 1708–1725. https://doi.org/10.1029/2018MS001313

Received 5 MAR 2018
Accepted 8 MAY 2018
Accepted article online 29 MAY 2018
Published online 31 JUL 2018

Abstract The atmospheric energy budget has recently been shown to provide powerful constraints on the position and shifts of the zonal and annual mean intertropical convergence zone (ITCZ), which lies close to the latitude of zero vertically integrated energy transport (energy flux equator, EFE). Relatively little work has, however, explored the applicability of the energetic framework to ITCZ shifts on shorter time scales. This study investigates to what extent the EFE tracks the ITCZ on subseasonal time scales in idealized aquaplanet simulations with different mixed layer depths. It is shown that the ITCZ always lags the EFE, even in the simulation with the shallowest mixed layer depth, making it possible for the EFE and the ITCZ to reside on opposite sides of the equator. At these times, which occur as the winter cross-equatorial Hadley circulation retreats from the summer hemisphere, the required energy balance is achieved not through shifts of the Hadley cell's ascending branch and ITCZ to track the EFE but through changes in the cell's vertical structure into one of negative gross moist stability. For any given position of the ascending branch, the winter cell is much weaker as it retreats from than as it expands into the summer hemisphere and develops a shallow return flow at middle-to-lower tropospheric levels where the moist static energy reaches its minimum, hence favoring a negative gross moist stability. It is argued that the asymmetry between the expanding and retreating phases of the winter Hadley cell is linked to the nonlinear seasonal evolution of near-surface temperatures.

1. Introduction

The most intense rainfall over the Earth's surface occurs within the intertropical convergence zone (ITCZ), a zonally elongated band of moist convection and low-level wind convergence over near-equatorial regions. In its annual and zonal mean, the ITCZ is located at around 6°N in present-day climate, with seasonal migrations characterized by a more northward (southward) position in boreal (austral) summer (e.g., Adler et al., 2003; Waliser & Gautier, 1993). Such asymmetry cannot arise from the insolation forcing, which is essentially symmetric about the equator. Hence, other asymmetries in the climate system must be responsible for the northward position of the ITCZ, such as possibly the coastline orientation of the Americas and feedbacks between resulting sea surface temperature (SST) patterns and low clouds (e.g., Philander et al., 1996) and the presence of the Andes (e.g., Takahashi & Battisti, 2007). Which asymmetry is the most relevant one remains a topic of active research, but consensus is emerging that the ocean meridional overturning circulation significantly contributes to the hemispheric asymmetry in tropical rainfall by transporting energy from the Southern Hemisphere (SH) to the Northern Hemisphere (NH; e.g., Frierson et al., 2013; Marshall et al., 2013).

Traditional theories have historically linked the ITCZ to tropical SSTs and associated gradients (e.g., Lindzen & Nigam, 1987; Sobel, 2007). However, modeling studies (e.g., Broccoli et al., 2006; Chiang et al., 2003; Vellinga & Wood, 2002; Yoshimori & Broccoli, 2008; Zhang & Delworth, 2005) and paleoevidence (e.g., Arbuszewski et al., 2013; Haug, 2001; Lea, 2003) suggest that the ITCZ responds strongly to extratropical thermal forcing, shifting into (away from) the relatively warmed (cooled) hemisphere. In the past decade, the vertically integrated atmospheric energy budget has provided the theoretical framework to understand the ITCZ response to remote forcing as part of the anomalous meridional energy fluxes needed to restore energy balance (e.g., Donohoe et al., 2013; Frierson & Hwang, 2012; Kang et al., 2008, 2009).

This framework has emphasized the anticorrelation between the ITCZ position and the cross-equatorial atmospheric energy transport and has led to the introduction of the energy flux equator (EFE, the latitude at which the meridional energy transport vanishes) as a diagnostic for the ITCZ (Kang et al., 2008). Central to these arguments is the assumption that in the tropics energy and moisture transports are primarily accomplished

by the Hadley circulation and that energy is transported in the direction of the Hadley cell's upper branch. Therefore, a northward (southward) shift of the ITCZ is associated with anomalous southward (northward) energy transport across the equator. The anticorrelation between the ITCZ and the cross-equatorial energy transport has been shown to be robust across observational data (e.g., Mcgee et al., 2014) and model experiments, with the ITCZ position being directly influenced by energetic perturbations (such as those associated with changes in ice albedo, clouds, and aerosols) in the extratropics (e.g., Frierson & Hwang, 2012; Hwang et al., 2013; Kang et al., 2008, 2009).

Factors controlling the sensitivity of the ITCZ position to the cross-equatorial energy transport are more directly quantified in Bischoff and Schneider (2014), who show how this sensitivity depends on the net energy input (NEI) into the equatorial atmosphere, that is, the net radiative fluxes at the top of atmosphere (TOA) minus any energy that is being uptaken by the ocean. This work emphasizes how changes in NEI near the equator can cause shifts in the ITCZ even without any change in cross-equatorial energy transport. Changes in NEI for instance explain the equatorward shift of the ITCZ during El Niño years.

While these energetic constraints have been shown to provide insight into the dynamics of annual and zonal mean ITCZ shifts, relatively little work has explored their implications on shorter time scales (e.g., subseasonal; (e.g., Adam et al., 2016a, 2016b; Chiang & Friedman, 2012; Donohoe et al., 2013). Adam et al. (2016a) use reanalysis data to show how the zonal mean EFE and the ITCZ position covary on time scales of seasons and longer. Interestingly, a lag between the EFE and the ITCZ exists, especially as the ITCZ moves from the NH to the SH. This lag is also seen in sector mean quantities over most ocean basins (Adam et al., 2016b). That is, there are times during the seasonal cycle when the EFE and the ITCZ can be on opposite sides of the equator, and hence, the vertically integrated energy transport and the mass transport in the upper branch of the Hadley circulation have opposite signs. These results therefore suggest limitations of the energetic perspective when considering ITCZ migrations on time scales shorter than seasonal and warrant further investigation.

This is indeed the scope of this paper. In particular, we want to address the following questions: (1) To what extent does the EFE track the ITCZ location on time scales shorter than seasonal? (2) Does a lag exist between these two quantities, and if so, how is this lag influenced by the heat capacity of the underlying ocean surface? (3) What are the implications of oppositely signed energy and mass transport (or negative gross moist stability, GMS) for the atmospheric tropical circulation? To highlight fundamental mechanisms in a model of minimal complexity and advance conceptual understanding, we will address these questions in idealized aquaplanet simulations that lack any zonal asymmetry.

The model and experimental design are described in section 2. In section 3, we discuss energetic constraints on the ITCZ position for summertime averages. ITCZ seasonal migrations and their relation to the cross-equatorial energy transport and the EFE are presented in section 4. There, possible mechanisms for the breakdown of commonly discussed relationships between the ITCZ, the EFE and the cross-equatorial energy transport are also discussed. We conclude in section 5 with a discussion and summary of our results.

2. Methods

2.1. Model and Experimental Design

We use an idealized general circulation model (GCM), which builds on the model of Frierson et al. (2006, 2007) and O'Gorman and Schneider (2008) and has been used in many studies of tropical and extratropical large-scale circulations (e.g., Bordoni & Schneider, 2008; Kaspi & Schneider, 2013; Merlis et al., 2013). The model is a primitive equation model of an ideal-gas atmosphere built on the Geophysical Fluid Dynamics Laboratory Flexible Modeling System. The primitive equations are solved spectrally at T42 horizontal resolution with 30 uneven sigma levels in the vertical. The radiation scheme is a two-stream radiative transfer scheme with gray atmosphere and prescribed optical thickness in longwave radiation. The GCM contains idealized representations of the effects of latent heat release on the dynamics, through a grid-scale condensation scheme and a quasi-equilibrium convection scheme (Frierson, 2007). Once liquid water is formed, it is immediately precipitated out; hence, there is no representation of clouds and cloud radiative feedback. Similarly, the prescribed optical depth in the radiation scheme is decoupled from the specific humidity; hence, there is no interactive water vapor feedback. The lower boundary consists of a uniform slab ocean of constant mixed layer depth. The idealized treatment of the physics and the idealized settings allow us to study the fundamental interaction between larger-scale circulations and moist convection in the absence of many complex and poorly constrained feedbacks, such as clouds.

Unlike previous studies of ITCZ dynamics using the same GCM (e.g., Bischoff & Schneider, 2014), here we perform simulations with a seasonal cycle of insolation with 360 days but no diurnal cycle. Orbital parameters are chosen to a near-contemporary obliquity of 23.5° and zero eccentricity. We choose a uniform mixed layer depth of 20 m, as representative of oceanic thermal inertias (Aqua20m). Sensitivity to the slab ocean depth is explored by conducting experiments with 10- (Aqua10m) and 0.2-m (Aqua0.2m) mixed layer depths. All simulations are started from an equilibrated equinoctial state and then integrated for 25 simulated years. Results are averaged over the last 15 simulated years. All statistics (including eddy fluxes) are computed from 6-hourly outputs and averaged at pentad (5 days) temporal resolution.

2.2. ITCZ and Energetic Diagnostics

In its most basic definition, the ITCZ is the locus of maximal tropical precipitation, $\phi_{P_{\max}}$. When applied to any precipitation field (either from model outputs or observations), this ITCZ indicator has two limitations. First, given that $\phi_{P_{\max}}$ is constrained by the horizontal resolution of the precipitation field, tracking seasonal migrations of the ITCZ using this indicator might introduce artificial discontinuities. Additionally, for situations where tropical precipitation features more than one peak, as commonly seen in both observations and model simulations (e.g., Lin, 2007; Zhang, 2001), seasonal precipitation redistributions between these peaks can introduce jumps or discontinuities in otherwise smooth precipitation changes.

Other ITCZ indices have therefore been introduced in the literature, such as the precipitation centroid of Frierson and Hwang (2012). More generally, Adam et al. (2016a) derive different ITCZ metrics using an integer power N of the area-weighted tropical precipitation:

$$\phi_{P_{\max,\mathrm{smth}}} = \frac{\int_{\phi_1}^{\phi_2} \phi[\cos\phi P]^N \mathrm{d}\phi}{\int_{\phi_1}^{\phi_2} [\cos\phi P]^N \mathrm{d}\phi}, \tag{1}$$

where P is the precipitation and ϕ the latitude. While $N = 1$ is the precipitation centroid, here we use $N = 10$, which, as discussed in Adam et al. (2016a), provides estimates of the ITCZ latitude that are close to the actual precipitation maximum but smooth out discretization issues. The integration boundaries ϕ_1 and ϕ_2 are chosen to cover the latitudinal span of tropical rainbands.

No single ITCZ indicator based on precipitation performs uniformly well across our simulations, which show a wide range of ITCZ structures, ranging from a well-defined single ITCZ in the Aqua20m case to a double ITCZ in the Aqua0.2m case, where a near-equatorial secondary precipitation maximum exists in the summer hemisphere during the warm seasons in addition to the seasonally moving convergence zone associated with the ascending branch of the Hadley cell (Figure 1). More specifically, while $\phi_{P_{\max,\mathrm{smth}}}$ faithfully tracks the precipitation maximum in the Aqua20m single ITCZ, its relation to the seasonally migrating convergence zone in the more extreme Aqua0.2m case is dubious (Figure 1d). For these reasons, while the ITCZ location ($\phi_{P_{\mathrm{ITCZ}}}$) is identified as $\phi_{P_{\max,\mathrm{smth}}}$ in Aqua20m, in Aqua10m, and Aqua0.2m, we identify it as the latitude of the poleward precipitation peak ($\phi_{P_{\max}}$) even at those few pentads during the seasonal cycle when the near-equatorial convergence zone has higher precipitation.

Given that the ITCZ is associated with the ascending branch of the tropical overturning circulation, it is also of interest to compare the ITCZ location with the dividing boundary between the two Hadley cells, that is the latitude where the meridional mass stream function vanishes ($\phi_{\psi=0}$). In the annual average or around the equinoxes, when the tropical overturning circulation is characterized by two cells that are almost symmetric about the equator, the ITCZ and the latitude at which the meridional mass stream function changes sign are expected to be collocated. Around solstices, however, when this equinoctial pattern is replaced by a solstitial pattern characterized by a strong, cross-equatorial winter cell and a much weaker, or negligible, summer cell, $\phi_{\psi=0}$ more clearly identifies the poleward boundary in the summer hemisphere of the winter cell (e.g., Privé & Plumb, 2007) and becomes progressively separated from the ITCZ, which is located equatorward of it (e.g., Lindzen & Hou, 1988). This is because precipitation is more directly linked to the region of strongest vertical velocity and hence of maximal meridional gradient of the mass flux stream function, which does not always coincide with the boundary between the two Hadley cells. We diagnose $\phi_{\psi=0}$ as the latitude at which the mass flux stream function reaches 5% of its maximum value, at the level of this maximum. This definition works well even when the circulation is dominated by the winter cell, with a negligible summer cell, and thus, the

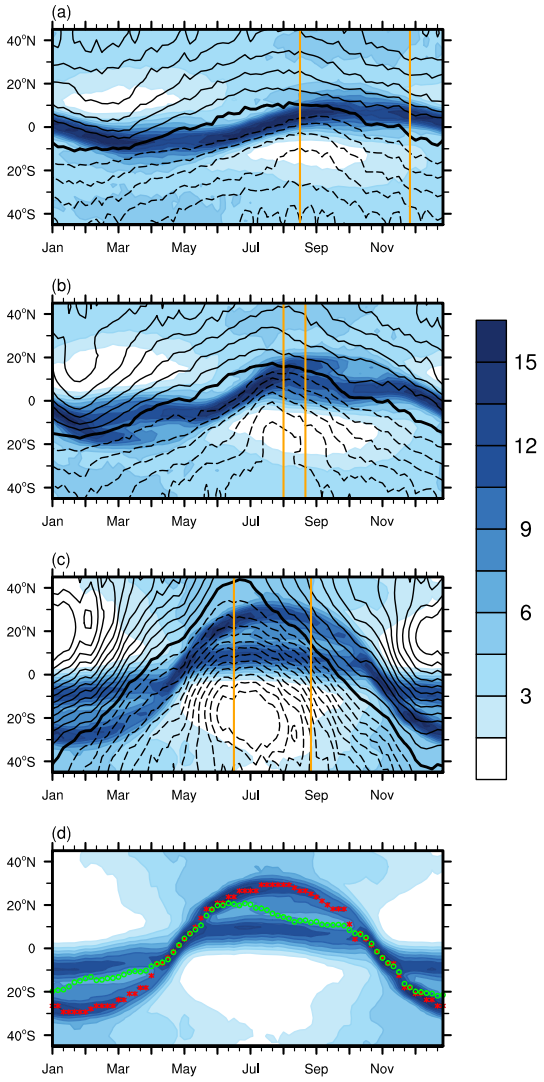

Figure 1. Seasonal evolution of zonal mean precipitation (shading, mm/day) and vertically integrated meridional energy flux (contours) in (a) Aqua20m, (b) Aqua10m, and (c) Aqua0.2m. The contour spacing is 2.5×10^7 W/m with solid contours for positive values, dashed contours for negative values, and thick contour for zero transport (energy flux equator). Vertical orange lines indicate the time period during which the intertropical convergence zone (ITCZ; $\phi_{P_{\mathrm{ITCZ}}}$) is poleward of 85% of its maximum excursion, which we use to construct summertime means in Figures 2 and 3. (d) Seasonal cycle of zonal mean precipitation in the Aqua0.2m simulation, as in (c). Red asterisks show $\phi_{P_{\mathrm{max}}}$ and the green open circles $\phi_{P_{\mathrm{max,smth}}}$. The integration boundaries ϕ_1 and ϕ_2 to calculate $\phi_{P_{\mathrm{max,smth}}}$ (equation (1)) are chosen as 35°S and 35°N for all three simulations, to account for the more extreme off-equatorial ITCZ excursions in the Aqua0.2m simulation.

boundary between the two Hadley cells becomes less well defined and cannot be diagnosed from a change in sign of the stream function (e.g., Faulk et al., 2017; Walker & Schneider, 2005).

Finally, we use the EFE, which, as discussed in section 1, has been shown to be a good predictor of the ITCZ and its response to perturbations for annual and zonal averages. The ϕ_{EFE} is defined as the latitude at which the vertically integrated meridional moist static energy (MSE) flux goes to 0:

$$\langle \overline{vh} \rangle_{\phi_{\mathrm{EFE}}} = 0, \tag{2}$$

where $\langle \cdot \rangle = \int_0^{p_s} (\cdot) \mathrm{d}p/g$ is a mass-weighted vertical average, $\overline{(\cdot)}$ represents time and zonal mean, and $h = C_p T + L_v q + gz$ is MSE. Assuming that the energy transport in the tropics is primarily effected by the Hadley circulation, the zero of the mass flux stream function, which is expected to covary with the ITCZ, will also be where the energy flux vanishes. In addition to diagnosing the location of the EFE directly from our simulations

as the latitude where the energy flux goes to zero (which in the following we will denote as $\phi_{\mathrm{EFE,actual}}$), we will also use the quantitative estimate of Bischoff and Schneider (2014). This estimate is obtained starting from the zonally averaged atmospheric energy budget:

$$\partial_t < \overline{\mathcal{E}} > = -\partial_y < \overline{vh} > + \overline{\mathcal{S}^t} - \overline{\mathcal{L}^t} + \overline{\mathcal{F}^s}, \tag{3}$$

where the left-hand side represents the atmospheric energy storage, with $\mathcal{E} = C_p T + L_v q$ and is approximately 0 for long time averages, and $\overline{\mathcal{S}^t} - \overline{\mathcal{L}^t} + \overline{\mathcal{F}^s}$ is the NEI, that is, the sum of TOA radiative fluxes (incoming shortwave radiation $\mathcal{S}^t$ minus outgoing longwave radiation $\mathcal{L}^t$) and upward surface fluxes ($\mathcal{F}^s$). For simplicity, here we express this equation in local Cartesian coordinates with $y = a\phi$ (where a is Earth's radius), but all calculations from the model outputs are done in spherical coordinates. Expanding the atmospheric energy flux around the equator to a first-order Taylor expansion in latitude (cf. Bischoff & Schneider, 2014), the latitude of the zero energy flux can be expressed as

$$\phi_{\mathrm{EFE,analytical}} \approx -\frac{1}{a} \frac{\langle \overline{vh} \rangle_0}{\overline{\mathcal{S}_0^t} - \overline{\mathcal{L}_0^t} + \overline{\mathcal{F}_0^s}}, \tag{4}$$

where the subscript 0 indicates quantities evaluated at the equator. This derived EFE latitude, which we refer to as the *analytical EFE*, is proportional to the cross-equatorial energy flux and inversely proportional to the NEI at the equator.

3. Summertime Means

The simulated seasonal cycle of the zonal mean precipitation is shown in Figure 1 for the three simulations with different mixed layer depths. In all simulations, tropical precipitation tends to be concentrated along narrow convergence zones that migrate seasonally across the equator into the summer hemisphere. Despite these broad similarities, important differences are observed: (1) With decreasing mixed layer depths, tropical precipitation shows a decreasingly lagged response to the imposed insolation, which reaches its maximum in the NH on 21 June (NH summer solstice); (2) with decreasing mixed layer depths, the ITCZ has larger seasonal excursions away from the equator (~8° in Aqua20m and ~30° in Aqua0.2m); (3) as the mixed layer depth is decreased, we see the appearance of a secondary precipitation band in the summer hemisphere that remains close to the equator throughout the warm season (Figures 1b and 1c). The zero meridional mass stream function tracks the surface MSE maximum in all simulations (shown in Figure 7 for Aqua20m) and covaries with the precipitation maximum, as expected from convective quasi-equilibrium theories for monsoon location (e.g., Emanuel, 1995; Privé & Plumb, 2007). The fact that a lagged response to the seasonal cycle of insolation exists even for a very shallow mixed layer depth indicates the importance of dynamic and thermal atmospheric inertia for the circulation and precipitation seasonal evolution.

Before investigating energetic constraints on the ITCZ position on subseasonal time scales, here we first focus on seasonal (summertime) averages. In particular, we consider NH summer and, to account for the different precipitation and circulation responses in simulations with different mixed layer depths (Figures 1a–1c), we perform averages around times of largest precipitation shifts (rather than averages around NH summer solstice). More specifically, we compute averages over the time period during which the ITCZ ($\phi_{P_{\mathrm{ITCZ}}}$) is poleward of 85% of its maximum excursion, as indicated within the orange lines in Figures 1a–1c. The resulting averaged stream function and precipitation are shown in Figures 2a, 2c, and 2e. Differences in the seasonal ITCZ migrations in the three simulations are reflective of differences in the seasonal cycle of the tropical overturning circulation and associated ascending branch. As the mixed layer depth becomes shallower, the summertime circulation is increasingly dominated by one single, strong winter Hadley cell that becomes progressively more and more cross equatorial. While this pattern is not representative of summertime conditions of the zonally averaged Hadley cell observed on Earth, it has been shown to be relevant for the dynamics of sector-averaged overturning circulations associated with monsoons (e.g., Bordoni & Schneider, 2008; Merlis et al., 2013).

Figure 3 shows the NH summertime averaged precipitation and vertically integrated total energy transport in the three simulations. The actual EFE is shown by the green circle, while the analytical EFE is shown by the red arrow. When considering summertime averages, both the actual and the analytical EFE show excellent skills in capturing the location of the precipitation maximum and, therefore, the poleward boundary in the summer hemisphere of the cross-equatorial cell (Figures 2a, 2c, and 2e). As we will discuss in the next session, this does not always hold true when the full seasonal cycle is being considered.

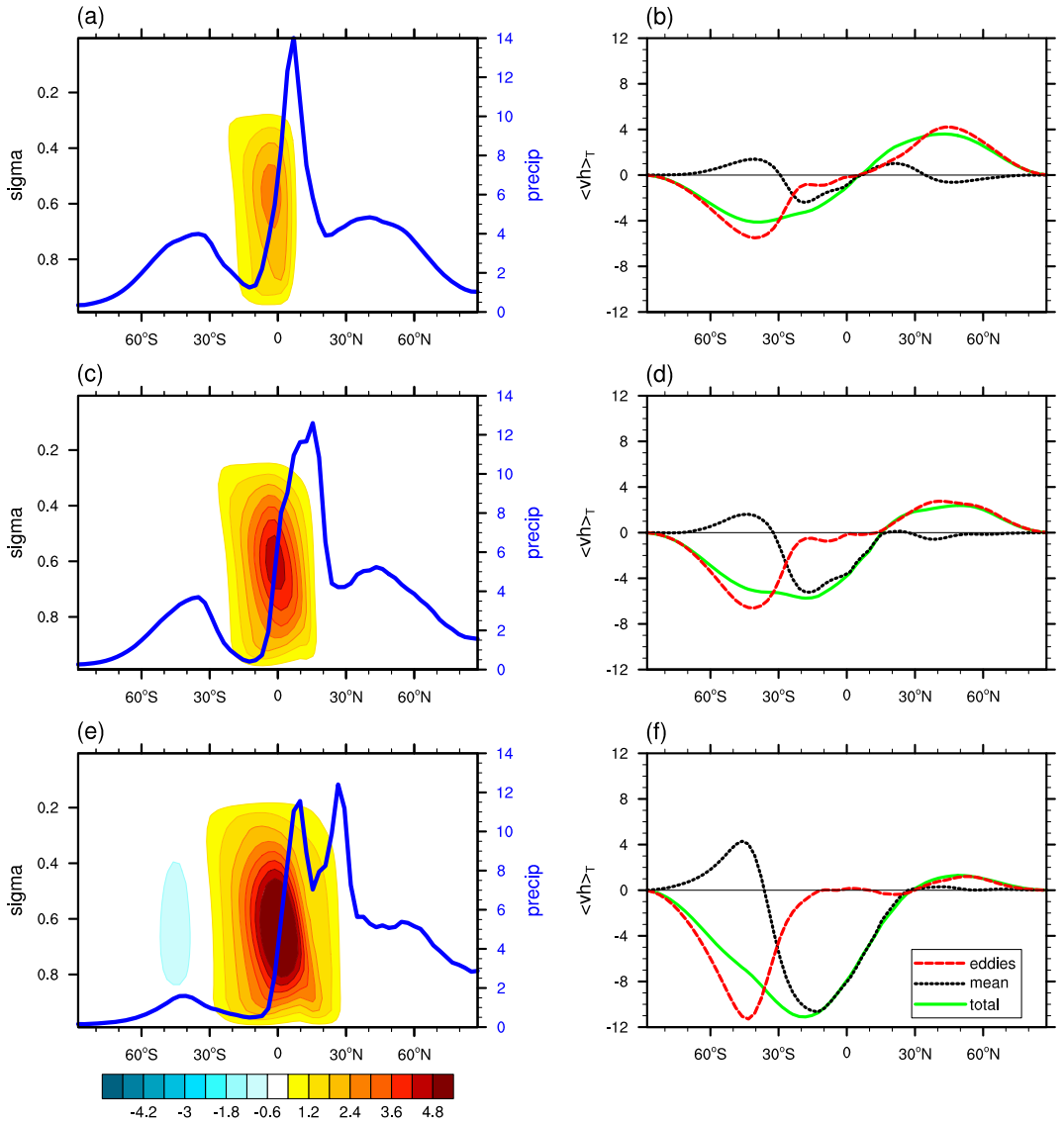

Figure 2. (a, c, and e) Summertime mean meridional stream function (shading, 10^{11} kg/s) and precipitation (blue line, right axis, mm/day) and (b, d, and f) energy transport for Aqua20m, Aqua10m, and Aqua0.2m, respectively. In (b), (d), and (f), total energy transport is shown in green, mean energy transport in black, and eddy energy transport in red.

The approximate colocation between the EFE and the ITCZ is also based on the assumption that in the tropics the energy transport is primarily effected by the mean meridional circulation (i.e., the Hadley cell). For a typical annual mean pattern of two Hadley cells almost symmetric about the equator, the cell's ascending branch, which is where the ITCZ resides, is also where the mean energy, mass, and moisture transports vanish. However, the energy balance more directly constrains the total, rather than the mean, energy transport, which justifies the identification of the EFE with the latitude at which the total transport goes to zero taken by many previous studies (e.g., Adam et al., 2016a; Bischoff & Schneider, 2014). This, however, raises the question of how the total transport is decomposed into mean and eddy contributions, and to what extent latitudes of EFE estimated from mean and total transports coincide.

This decomposition is shown in Figures 2b, 2d, and 2f. For the Aqua20m experiment, we find that while the mean transport dominates in the stronger winter cell, the eddy transport is comparable to the mean transport in the weaker summer cell; this configuration is similar to what observed on Earth for the zonal mean ITCZ. In this case, although the eddy transport is not negligible, total, mean, and eddy transports all vanish at the same location. In Aqua0.2m and Aqua10m, where the asymmetry between the winter and summer cells is

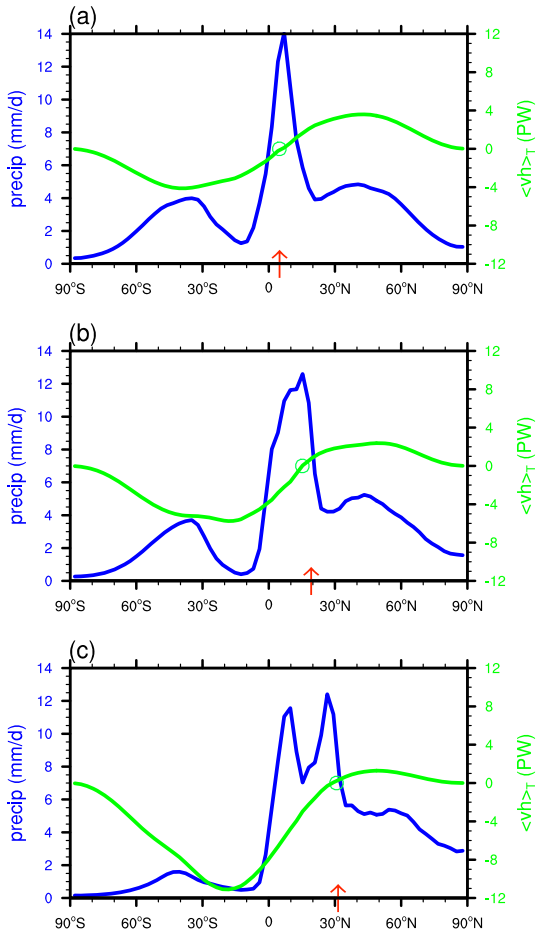

Figure 3. Summertime zonal mean precipitation (blue) and vertically integrated energy transport (green) in (a) Aqua20m, (b) Aqua10m, and (c) Aqua0.2m. The green circles are $\phi_{EFE,actual}$ and the red arrows $\phi_{EFE,analytical}$.

much stronger than in the Aqua20m case, we see that because there is no significant positive mean transport in the summer cell, the poleward boundary of the winter Hadley cell does not coincide with the latitude at which the mean energy transport switches sign (i.e., there is no clear mean EFE). Rather, the dividing boundary between southern and northern cells is the latitude where the total energy transport transitions from being effected by the mean in the winter cell (with negligible contribution by the eddies) to being primarily effected by the eddies in the weaker and entirely eddy-driven summer cell (e.g., Schneider & Bordoni, 2008; Singh et al., 2017; Walker & Schneider, 2006). This pattern is in disagreement with the conventional picture of a weakly cross-equatorial Hadley cell, in which the mean energy transport in the two cells is comparable in magnitude and of opposite sign, and the mean EFE coincides with the ITCZ. In this pattern, in fact, not only is the eddy energy transport not negligible in the proximity of the ITCZ, but also a mean EFE cannot always be identified. This confirms that in general the total EFE is a better predictor of the ITCZ location than the mean EFE. For this reason, for the rest of this paper we will focus on the total EFE and explore its relation to the ITCZ location throughout the seasonal cycle.

4. Seasonal Migrations

4.1. Lag Between the EFE and the ITCZ

One interesting feature emerging from Figures 1a–1c is that the EFE (thick black lines) always leads the precipitation maximum, even when the mixed layer depth is very shallow. While some previous studies have shown a similar lead-lag relationship in observations and modeling studies, no explanation of this seasonal offset has been offered. That the ϕ_{EFE} leads the $\phi_{P_{ITCZ}}$ can also be seen in a scatter plot of their seasonal evolution (Figure 4a). The two quantities are correlated in all simulations, with correlation coefficients of 0.48, 0.72 and 0.84 in Aqua20m, Aqua10m, and Aqua0.2m, respectively. However, the existence of a lag between

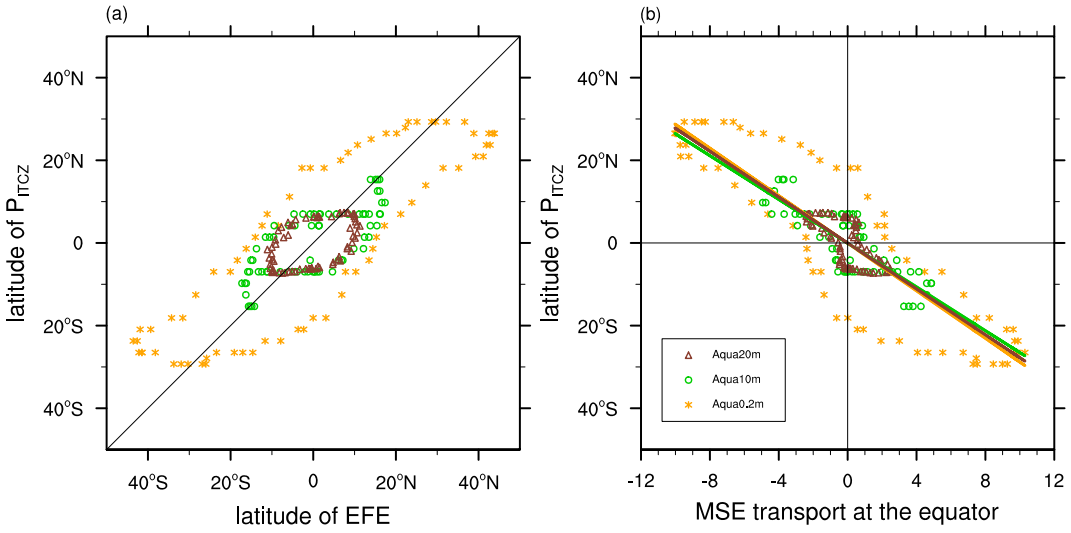

Figure 4. Scatter plot of the seasonal cycle of (a) $\phi_{P_{ITCZ}}$ versus $\phi_{EFE,actual}$ and (b) $\phi_{P_{ITCZ}}$ versus cross-equatorial energy transport in Aqua20m (brown open triangles), Aqua10m (green open circles), and Aqua0.2m (orange asterisks). The slopes in (b) are −2.77°/PW for Aqua20m, −2.65°/PW for Aqua10m, and −2.87°/PW for Aqua0.2m. ITCZ = intertropical convergence zone; MSE = moist static energy; EFE = energy flux equator.

the two quantities leads to an elliptical pattern rather than a straight line. Also, while the slope between the ϕ_{EFE} and the $\phi_{P_{ITCZ}}$ is close to one in all simulations, the ϕ_{EFE} tends to be poleward of the $\phi_{P_{ITCZ}}$. This is especially evident in the Aqua0.2m simulation and is a result of the latitudinal separation between the EFE and the ITCZ in strongly cross-equatorial Hadley cells (e.g., Faulk et al., 2017). Given that many previous studies have more directly related the ITCZ to the cross-equatorial energy transport, we also plot the scatter plot of the seasonal evolution of $\phi_{P_{ITCZ}}$ and cross-equatorial energy transport (Figure 4b). Seasonal variations of $\phi_{P_{ITCZ}}$ and cross-equatorial energy transport are strongly anticorrelated with a slope of around −2.76°/PW (with correlation coefficients of 0.66, 0.81, and 0.88 in Aqua20m, Aqua10m, and Aqua0.2m, respectively), and have a time offset relative to each other. While the regression coefficient between the ITCZ location and the cross-equatorial energy transport in our simulations is similar to what seen in observations (−2.7°/PW, Donohoe et al. (2013)), we find that it remains roughly constant with decreasing mixed layer depth, unlike what was argued in their paper. The reason of this discrepancy is unclear, but it might arise from the lack of cloud and other radiative feedbacks in our idealized model. Additionally, the sensitivity of the ITCZ location to changes in cross-equatorial energy transport is not constant throughout the year, but has a semiannual component, primarily arising through seasonal changes in the NEI into the equatorial atmosphere (equation (4)). Consistent with arguments in Donohoe et al. (2013), this leads to a flatter slope between the ITCZ location and the cross-equatorial energy transport at times of maximal off-equatorial excursions.

In order to quantify more directly the seasonal evolution of the ITCZ, the circulation, and the EFE, here we define their seasonal amplitude and phase as the amplitude and phase of the annual harmonic of the ITCZ

Table 1
Amplitude and Phase of the Annual Cycle of the $\phi_{P_{ITCZ}}$, $\phi_{\psi=0}$, and ϕ_{EFE} in the Aqua20m, the Aqua10m, and Aqua0.2m Simulations

	Amplitude (degree)			Phase (day)		
	Aqua0.2m	Aqua10m	Aqua20m	Aqua0.2m	Aqua10m	Aqua20m
$\phi_{P_{ITCZ}}$	30.19	10.56	7.59	121.83	162.47	197.26
$\phi_{\psi=0}$	32.11	17.59	11.41	118.03	159.12	184.55
ϕ_{EFE}	37.53	15.45	10.46	90.76	122.38	136.52
δphase ($\phi_{P_{ITCZ}} - \phi_{EFE}$)				31.07	40.09	60.74

Note. The phase shown here is the day of the crest of the annual cycle relative to the time of equinoctial insolation on 21 March. The last row shows the phase difference between $\phi_{P_{ITCZ}}$ and ϕ_{EFE}.

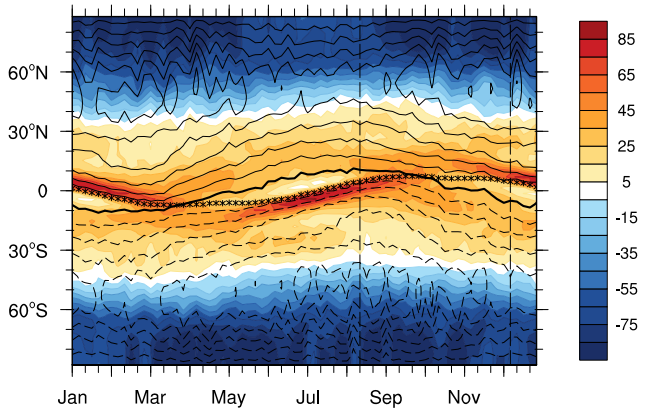

Figure 5. Seasonal cycle of the zonal mean effective net energy input (NEI_{eff}, shading, W/m^2) and vertically integrated meridional energy flux (contours, interval 2.5×10^7 W/m) in Aqua20m. Asterisks show $\phi_{P_{ITCZ}}$. Vertical black dashed lines indicate pentads 11–15 August and 6–10 December, respectively, which are chosen as times in which the southern winter cross-equatorial Hadley cell is expanding into and retreating from the northern summer hemisphere (as shown in Figures 8a and 8b) but has the same ITCZ location.

position ($\phi_{P_{ITCZ}}$), the location of the zero stream function ($\phi_{\psi=0}$), and the EFE ($\phi_{EFE,actual}$). Corresponding values are shown in Table 1. It is evident that for all simulations the EFE leads the ITCZ, with the lead decreasing from about 2 months in Aqua20m to about 1 month in Aqua0.2m. In general, the circulation boundary and the ITCZ tend to evolve more closely in phase during the seasonal cycle.

These results raise a number of questions: (1) Why does the EFE always lead the ITCZ, even in the limit of very small thermal inertia of the lower boundary? (2) To the extent that precipitation might be more strongly constrained by the mass and moisture budgets than the energy budget on seasonal time scales, can we offer any insight on when and how the EFE fails as a diagnostic of the ITCZ during the seasonal cycle?

As discussed throughout this paper, energetic constraints on the ITCZ location have emphasized the anticorrelation between the cross-equatorial energy transport and the position of the ITCZ, with the ITCZ shifting into the warmer hemisphere (i.e., the summer hemisphere during the seasonal cycle) and energy being transported into the cooler hemisphere (i.e., the winter hemisphere) in the same direction as the Hadley cell's upper branch. One important assumption is that the effective energy stratification, or GMS, of the Hadley cell, which is defined in this study as $\mathrm{GMS} = \int_0^{p_s} \overline{vh}\frac{dp}{g} / \int_0^{p_m} \bar{v}\frac{dp}{g}$, where p_m is the pressure at maximum stream function, is positive (e.g., Feldl et al., 2017; Frierson, 2007; Hill et al., 2015; Kang et al., 2009). According to this definition, the GMS represents the energy transported per unit mass transport. With positive GMS, the vertically integrated energy transport and the mass transport in the cell's upper branch have the same sign, and the EFE is collocated with the boundary between the two Hadley cells (and hence is just slightly poleward of the ITCZ). Our simulations suggest that in the course of the seasonal cycle this does not always hold true. In fact, one important consequence of the lead-lag relationship between the EFE and the ITCZ is that there are times during the seasonal cycle when the EFE and the ITCZ are on opposite sides of the equator (e.g., around May to June and November to December), leading to a breakdown of the commonly assumed anticorrelation between the ITCZ and the cross-equatorial energy transport. More generally, this suggests that vertically integrated energy transport and upper-level mass transport at certain latitudes and times are in opposite directions, implying negative GMS of the corresponding Hadley cell. In the following, we want to investigate mechanisms of the lag relationship between the EFE and the ITCZ and changes in the circulation leading to negative GMS. We primarily focus on the Aqua20m simulation, which features the largest phase difference between the EFE and the ITCZ, and a Hadley cell structure and seasonality that is more similar to the zonally averaged circulation observed on Earth.

4.2. Seasonal Evolution of the EFE and the ITCZ Position

To understand why the EFE leads the ITCZ, it is useful to go back to the energy budget and understand what determines the phase of the annual cycle of the ϕ_{EFE}. At each given latitude, the total energy transport in petawatts (PW) can be expressed as follows:

$$\langle\overline{vh}\rangle_{T,\phi} = 2\pi\int_{SP}^{\phi}\partial_y\langle\overline{vh}\rangle\cos\phi a^2\mathrm{d}\phi = 2\pi\int_{SP}^{\phi}\mathrm{NEI}_{\mathrm{eff}}\cos\phi a^2\mathrm{d}\phi, \tag{5}$$

where we start the integration from the South Pole (SP) where there is no energy transport, a is the radius of the Earth, subscript T is used to emphasize that this quantity represents the energy transport in units of petawatt, and $\mathrm{NEI}_{\mathrm{eff}}$ is the effective NEI, which is equal to NEI minus the atmospheric storage ($\partial_t\langle\overline{\mathcal{E}}\rangle$). In Aqua20m, the atmospheric energy storage term is negligible in the energy balance equation (cf. equation (3)) on seasonal time scales, so the divergence of the energy transport itself is approximately equal to the NEI into the atmospheric column at each given pentad. However, the seasonal distribution of the storage term does have nonnegligible contributions to the total meridional energy transport, as will be shown below.

Based on equations (2) and (5), the EFE is the latitude at which the meridionally integrated energy input to its north and south is the same and equal to 0:

$$\begin{aligned}\langle\overline{vh}\rangle_{T,\phi_{\mathrm{EFE}}} &= 2\pi\int_{SP}^{\phi_{\mathrm{EFE}}}\mathrm{NEI}_{\mathrm{eff}}\cos\phi a^2\mathrm{d}\phi\\ &= 2\pi\int_{\phi_{\mathrm{EFE}}}^{NP}\mathrm{NEI}_{\mathrm{eff}}\cos\phi a^2\mathrm{d}\phi\\ &= 0.\end{aligned} \tag{6}$$

This is to say that the EFE, rather than being collocated with maximum energy flux divergence as it is often the case for the precipitation maximum, is determined by the meridional integral of the NEI. The relationship between the seasonal evolution of the EFE and the $\mathrm{NEI}_{\mathrm{eff}}$ is made more apparent in Figure 5: While there are regions of localized $\mathrm{NEI}_{\mathrm{eff}}$ maxima, which indicate maximum divergence near the ITCZ, it is the hemispherically asymmetric distribution of the $\mathrm{NEI}_{\mathrm{eff}}$ in regions away from the precipitation (and hence $\mathrm{NEI}_{\mathrm{eff}}$) maxima that determines the seasonal evolution of the EFE. In other words, the overall seasonally evolving spatial pattern of $\mathrm{NEI}_{\mathrm{eff}}$ dictates the seasonal evolution of the EFE and its migration on either side of the equator, whereas its local structure more directly determines the divergence of the energy flux.

A more direct assessment of factors contributing to the seasonal evolution of the energy transport—and with it of the EFE—can be obtained through the following decomposition:

$$\langle\overline{vh}\rangle_{T,\phi} = \overbrace{2\pi\int_{SP}^{\phi}\partial_y\langle\overline{vh}\rangle\cos\phi a^2\mathrm{d}\phi}^{A} \tag{7}$$

$$= \underbrace{2\pi\int_{SP}^{\phi}\mathrm{NEI}\cos\phi a^2\mathrm{d}\phi}_{B} \underbrace{-2\pi\int_{SP}^{\phi}\partial_t\langle\overline{\mathcal{E}}\rangle\cos\phi a^2\mathrm{d}\phi}_{C} \tag{8}$$

$$\begin{aligned}&= \underbrace{2\pi\int_{SP}^{\phi}\overline{S^t}\cos\phi a^2\mathrm{d}\phi}_{B_1} \underbrace{-2\pi\int_{SP}^{\phi}\overline{\mathcal{L}^t}\cos\phi a^2\mathrm{d}\phi}_{B_2}\\ &\quad+\underbrace{2\pi\int_{SP}^{\phi}\overline{\mathcal{F}^s}\cos\phi a^2\mathrm{d}\phi}_{B_3} -2\pi\int_{SP}^{\phi}\partial_t\langle\overline{\mathcal{E}}\rangle\cos\phi a^2\mathrm{d}\phi,\end{aligned} \tag{9}$$

where the total energy transport (term A) is decomposed into contributions from the NEI (term B) and the storage term (term C). The NEI (integrand in term B) can be further decomposed into shortwave (integrand in term B_1) and longwave (integrand in term B_2) radiation at TOA, and surface fluxes (integrand in term B_3). The evolution of the seasonal anomaly (defined as the deviation from the annual mean at each latitude) of each term is shown in Figure 6, which suggests that it is the seasonal cycle of the shortwave radiation that contributes the most to the phase of the seasonal evolution of the energy transport.

More quantitatively, amplitude and phase of the annual harmonic of each term at 11°N is shown in Table 2. While the contributions from the NEI and the energy storage have similar seasonal amplitudes, the phase of

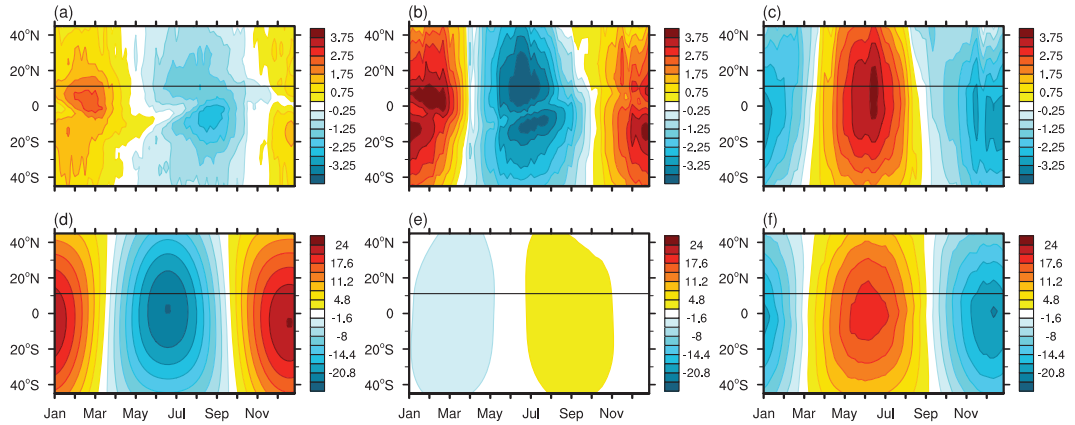

Figure 6. Seasonal evolution of the anomalous (relative to the annual mean) (a) vertically integrated energy transport (PW) and its decomposition into contributions from (b) net energy input, (c) negative atmospheric energy storage, (d) downward shortwave radiation at the top of atmosphere, (e) negative upward longwave radiation at the top of atmosphere, and (f) upward surface fluxes in Aqua20m. Thin black lines indicate 11°N, the location we choose to show phase and amplitude of all terms contributing to the vertically integrated energy transport in Table 2.

the total energy transport is primarily influenced by the phase of the NEI-derived energy transport. Among individual terms in the NEI, the contribution from $\mathcal{S}^t$ is the one that features the largest amplitude and the phase that best agrees with that of the NEI-derived and, hence, of the total energy transport. This implies that the seasonal migration of the EFE is almost in phase with the seasonally varying insolation forcing and that the atmospheric circulation needs to change to achieve the required energy flux and energy flux divergence. However, the atmospheric circulation, which is primarily constrained by surface thermodynamics, cannot adjust as rapidly as the EFE because of thermal and dynamic inertia. This is to say that the tropical precipitation nearly coevolves with surface temperature and surface MSE (e.g., Emanuel, 1995; Privé & Plumb, 2007) and, like these surface thermodynamic quantities, lags the insolation and the EFE (Figure 7b). The lag between the EFE and the Hadley cell's poleward extent and the associated ITCZ is thus shorter with decreasing mixed layer depths and thermal inertia of the lower boundary (e.g., Cronin & Emanuel, 2013; Dwyer et al., 2012). In summary, the lag between the EFE and the ITCZ is related to the lag between insolation and surface temperature. The phase offset between the EFE and the ITCZ, however, contradicts the assumption that the GMS of the Hadley cell is always positive, raising the question of how the circulation adjusts to achieve the required energy balance.

4.3. Circulation Response

To understand how the system achieves negative GMS at some latitudes and times during the seasonal cycle, we investigate how the circulation and the energy field evolve with time. We begin by showing in Figure 7 the evolution of the circulation boundary, the ITCZ, and the EFE. As discussed in the previous subsection, the phase of the annual cycle of the EFE is mainly determined by the solar insolation, while the circulation boundary and the precipitation maximum migrate with a lag; yet energy balance still needs to be satisfied. We therefore select two pentads (11–15 August and 6–10 December) at which the ITCZ is located at the same latitude in the NH (around 4.5°N), while the EFE sits in the NH (around 10.5°N) and SH (around 5°S), respectively. How do the corresponding Hadley cells differ at these two times to achieve oppositely directed energy transports near the equator while featuring ascending branches at approximately the same latitude? The mass flux stream functions at these two pentads (Figures 8a and 8b) show that the cross-equatorial cell is much stronger on 11–15 August than it is on 6–10 December, which highlights the existence of an asymmetry between the expanding and retreating phases of the cross-equatorial winter cell.

Table 2
Amplitude and Phase of the Annual Cycle of the Meridional Energy Transport at 11°N and of the Contributions to $\langle\overline{vh}\rangle_{T,\phi}$ From Each Term in Equations (7)–(9)

	Term A	Term C	Term B	Term B_1	Term B_2	Term B_3
$\langle\overline{vh}\rangle_{T,11°N}$ *Amplitude (PW)*	1.83	3.17	3.87	23.07	3.4	18.88
$\langle\overline{vh}\rangle_{T,11°N}$ Phase (day)	317.46	76.75	282.2	267.35	161.49	74.29

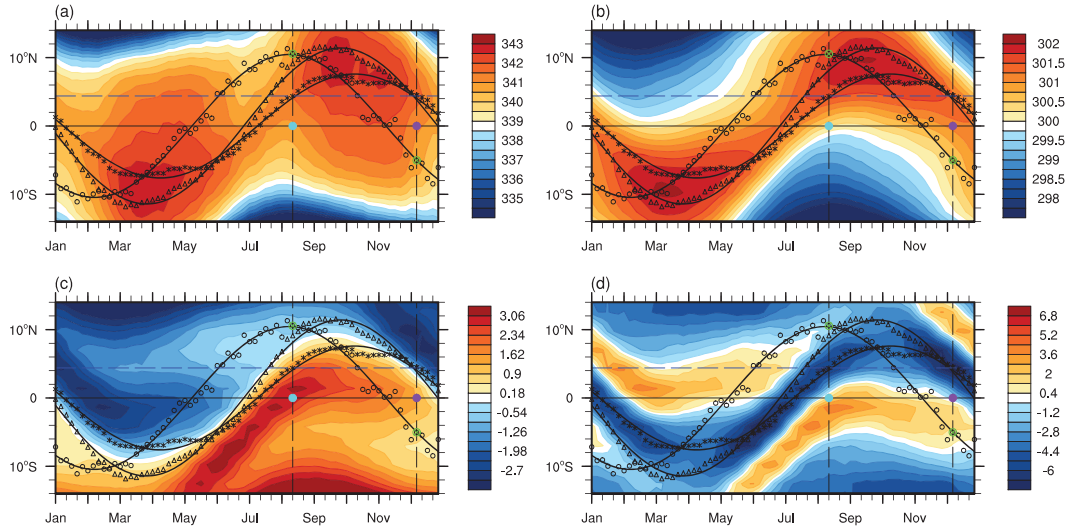

Figure 7. Seasonal evolution of the zonal mean (a) moist static energy (K), (b) temperature (K), (c) meridional gradient of temperature (10^{-6} K/m), and (d) Laplacian of temperature (10^{-12} K/m^2) at the lowest model level ($\sigma = 0.989$) in shading in Aqua20m. The open circles are $\phi_{\mathrm{EFE,actual}}$, the open triangles $\phi_{\psi=0}$, and the asterisks $\phi_{P_{\mathrm{ITCZ}}}$. Solid thick black lines show their annual harmonic. Vertical black dashed lines indicate pentads 11–15 August and 6–10 December, respectively, shown in Figure 5, which have the same ITCZ location, shown by the horizontal blue dashed line but different EFE, denoted by the green ⊗ symbol. The horizontal thin black line indicates the equator. The cyan and purple dots represent location (equator) and times (11–15 August and 6–10 December, respectively) for the vertical cross sections shown in Figures 8c and 8d.

To understand how oppositely signed cross-equatorial energy transport is effected at these two pentads, the corresponding vertical profiles of v and h at the equator are shown in Figures 8c and 8d, for the August and December pentad, respectively. The MSE vertical profiles at both pentads are consistent with observed typical profiles in the tropical atmosphere, with a minimum in the middle-to-lower troposphere and values at upper levels being larger than those close to the surface. While largely similar, these profiles differ in the lower atmosphere, with slightly higher MSE values below the minimum being found over a deeper layer in the retreating phase. Vertical profiles of the meridional wind, however, feature more pronounced differences. More specifically, in the retreating phase, the cross-equatorial Hadley cell develops a shallow return flow at heights where the MSE minimum is located. This is also evident in the structure of the stream function (Figure 8b). That the differences in the circulation (or meridional wind) vertical structure are more important than the differences in the MSE vertical structure for the sign reversal of the GMS in the retreating phase of the winter Hadley cell can be more accurately quantified by decomposing the anomalous mean MSE flux according to

$$\langle \delta(\bar{v}\bar{h}) \rangle = \langle \bar{v}\delta\bar{h} \rangle + \langle \bar{h}\delta\bar{v} \rangle, \tag{10}$$

where δ represents the difference between the December and August fields (6–10 December minus 11–15 August) and we neglect the quadratic term. The first term represents the contribution to the anomalous mean MSE flux due to changes in the MSE vertical profile, while the second term represents the contribution due to changes in the meridional wind vertical profile. As shown in Figure 9, in the tropics differences in the total MSE flux between the two pentads are almost entirely accounted for by differences in mean MSE flux, which in turn are primarily dominated by differences in the circulation vertical structure rather than differences in MSE profiles. In other words, it is the presence of the shallow return flow near the MSE minimum, rather than MSE increases at lower levels, that causes the vertically integrated energy transport to be in the direction of the lower-level mass transport in the retreating phase, resulting in a negative GMS. At other pentads, the retreating cell does not always feature a shallow return flow as well defined as that seen around 6–10 December. Nonetheless, the structure of the associated stream function is very different from that of the winter cell in its expanding phase, with the upper- and lower-level meridional flow being confined in very thin layers, which also favors negative GMS (not shown). This means that while the EFE evolves seasonally almost in phase with the insolation, the surface temperature, the Hadley cell, and its ascending branch cannot change as rapidly.

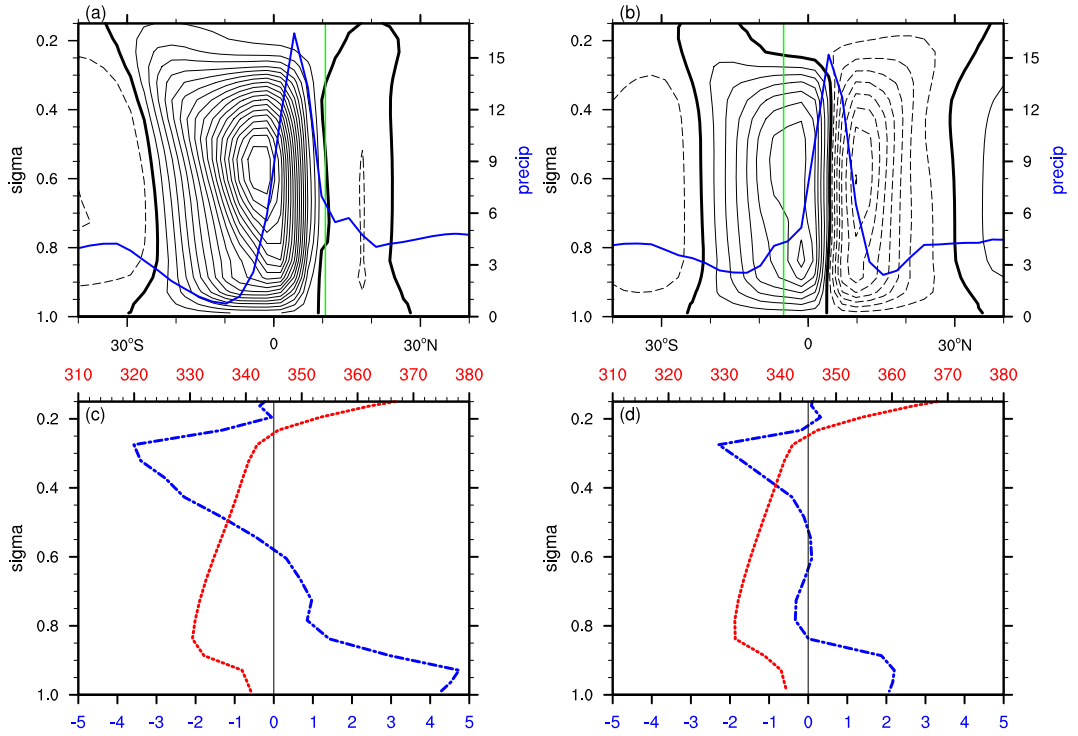

Figure 8. Meridional mass stream function (contours, interval 1.75×10^{10} kg/s) in Aqua20m for (a) 11–15 August and (b) 6–10 December. Solid (dashed) contours indicate positive (negative) values and the thick black contours the zero value. Blue solid line is zonal mean precipitation and the green vertical line indicates $\phi_{\mathrm{EFE,\ actual}}$. Vertical profiles of the MSE (red dotted line, K) and meridional wind (blue dash-dotted line, m/s) at the equator on (c) 11–15 August and (d) 6–10 December.

Without shifting the boundary between the two Hadley cells and the ITCZ across the equator together with the EFE, the Hadley cell achieves the required energy transport by changing its vertical structure into one with negative GMS.

An interesting question arising from this discussion is how the retreating cell develops the shallow return flow and why an asymmetry exists between the times at which the cross-equatorial Hadley cell (the southern cell for northern summer and the northern cell for southern summer) is expanding into and retreating from the summer hemisphere. Figure 7c shows that the meridional temperature gradient within the latitudinal span of the cross-equatorial Hadley cell is stronger when the cell is expanding than it is when retreating, which might

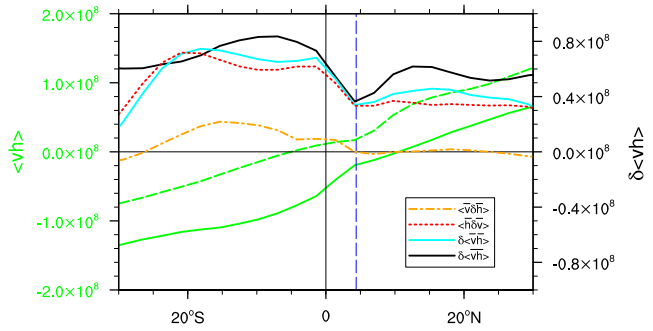

Figure 9. Meridional distribution of energy flux (W/m) on 11–15 August (solid green line) and 6–10 December (dashed green line, left y axis) and difference (6–10 December minus 11–15 August) between the two ($\delta\langle\overline{v}\overline{h}\rangle$, black solid line, right y axis). Anomalous mean energy flux ($\delta\langle\bar{v}\bar{h}\rangle$), and contributions from changes in meridional wind profile ($\langle\bar{h}\delta\bar{v}\rangle$) and from changes in moist static energy profile ($\langle\bar{v}\delta\bar{h}\rangle$) are shown in cyan solid line, red dashed line, and orange dash-dotted line, respectively (right y axis). The vertical blue dashed line indicates the latitude of the ITCZ ($\phi_{P_{\mathrm{ITCZ}}}$) at these two pentads.

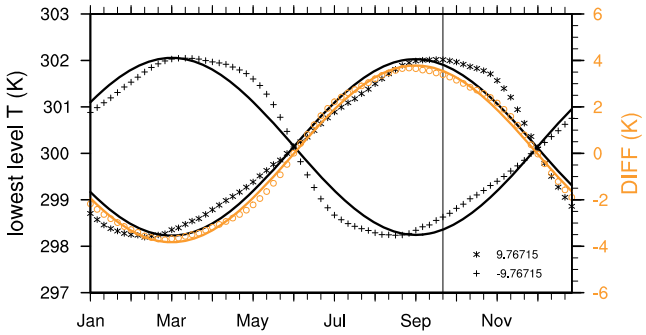

Figure 10. Seasonal evolution of the lowest level atmospheric temperature at around 10°N (black asterisks) and 10°S (black crosses) in Aqua20m. Orange open circles show the difference between these two, representative of the average meridional temperature gradient near the equator. Solid lines show their annual harmonic. The vertical black line indicates the time at which $\phi_{P_{\mathrm{ITCZ}}}$ has the largest northward excursion.

support a weaker overturning circulation in its retreating phase. We also find that the meridional Laplacian of temperature below the ITCZ is slightly more negative when the cell is retreating from the summer hemisphere (Figure 7d), suggestive of the role of boundary layer convergence in favoring bottom heavy vertical velocity profiles (e.g., Back & Bretherton, 2009; Lindzen & Nigam, 1987; Sobel, 2007). We therefore want to investigate the reasons for the asymmetry in the near-surface temperature evolution. We do so by plotting in Figure 10 the seasonal evolution of the near-surface temperature at 10°N (asterisks) and 10°S (crosses). It can be seen that in both hemispheres the near-surface temperature evolves more slowly as it is increasing and more rapidly as it is decreasing, resulting in a tilted sinusoidal evolution (i.e., the temperature evolution shifts to the right [left] of the sine wave when it is warmer [colder] than annual mean temperature). With opposite temperature seasonal anomalies and oppositely tilted temperature evolutions at 10°N and 10°S, the averaged meridional surface temperature gradient near the equator, approximated by the difference between the temperature at 10°N and 10°S, is stronger as the winter cross-equatorial cell is expanding (before the time at which NH temperature peaks and the precipitation reaches the location of its maximum northward excursion) than as it is retreating (after the time at which NH temperature peaks).

While the mechanisms responsible for the tilted temperature evolution remain unclear, they most likely involve nonlinearities in the effective heat capacity of the coupled atmosphere/slab ocean system and/or nonlinear circulation influences. These mechanisms will be explored in more detail in future work. Through its impact on the circulation, the asymmetry in the temperature evolution appears essential for the lead-lag

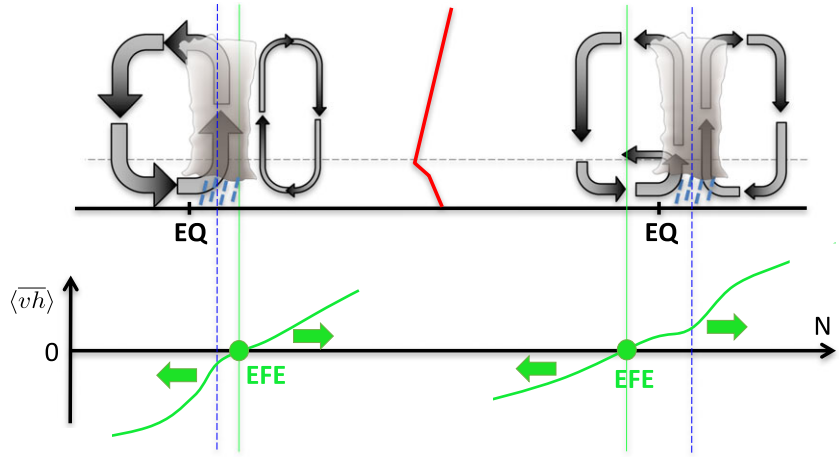

Figure 11. Schematic of the asymmetry between the expanding (left) and retreating (right) phases of the winter cross-equatorial cell for northern summer. The upper panel shows the structure of the overturning cell and associated ITCZ, and the vertical profile of moist static energy in red. The lower panel shows the meridional energy flux (green line) and the EFE (green dots). The vertical blue dashed lines indicate the ITCZ. EFE = energy flux equator.

relationship between the EFE and the ITCZ, as complete symmetry between expanding and retreating phases would imply cross-equatorial winter cells with equal mass and energy transports for any given ITCZ location. Hence, the EFE and the ITCZ would evolve in phase.

5. Discussions and Conclusions

In this study, we have explored the extent to which emerging energetic constraints on the ITCZ provide accurate predictions of its evolution on seasonal and shorter time scales in idealized aquaplanet simulations with different mixed layer depths. In agreement with previous studies, the EFE shows excellent skill in capturing the location of the precipitation maximum on seasonal or longer means. One important caveat is that it is the total, rather than the mean, EFE that provides the best ITCZ predictor across simulations. As the mixed layer depth decreases, the asymmetry between the winter and summer Hadley cell increases during the warm seasons, with the strong and broad winter Hadley cell approaching conservation of angular momentum and the weak and narrow summer cell being eddy driven (e.g., Schneider & Bordoni, 2008; Singh et al., 2017; Walker & Schneider, 2006). In this case, unlike what is usually assumed, not only is the eddy energy transport not negligible in the summer cell, but it determines the zero of the total energy flux even when the mean energy flux approaches zero but does not change sign. Hence, in these more asymmetric cases, the poleward boundary of the winter cell in the summer hemisphere, which is approximately collocated with the ITCZ, coincides with the latitude at which the total, and not the mean energy transport, switches sign as it transitions from being effected by the mean in the winter cell to being effected by the eddies in the summer cell.

On subseasonal time scales, we find that the EFE leads the ITCZ and the maximum in lower-level MSE. This arises because, while the seasonal evolution of the EFE is primarily in phase with the insolation changes, the circulation and associated precipitation more closely track the near-surface temperature and cannot adjust as rapidly. In fact, while decreasing with decreasing mixed layer depths, the lag is as large as about 1 month even for the shallowest depth. This implies that the seasonal evolution of the ITCZ is not simply negatively correlated with the strength of the cross-equatorial energy transport: There are times when the ITCZ and the EFE reside on opposite sides of the equator. It also implies that at these times, the GMS of the Hadley circulation is negative, with the overturning cell transporting energy in the direction of the lower-level, rather than upper-level, mass transport. These results therefore suggest that one important pathway by which the tropical circulation achieves the required energy balance in the seasonal cycle is through changes in the efficiency of its energy transport, that is the GMS, in addition to changes in its mass transport. This manifests as an asymmetry in the vertical structure of the winter cell in its expanding and retreating phases. For a given position of the ascending branch, the cell is much weaker as it retreats from than as it expands into the summer hemisphere and has the tendency to develop a shallow return flow at the levels in the middle-to-lower troposphere where the MSE reaches its minimum, favoring a negative GMS. Differences in the structure, energy transport, EFE, and ITCZ of the cross-equatorial Hadley cell in its expanding and retreating phases are schematically summarized in Figure 11 for northern summer.

While we do not have a theory for the development of such a shallow return flow within a circulation with a deep ascent, the asymmetry between the expanding and retreating phases of the winter cell seems to be linked to an asymmetry in the near-surface temperature seasonal distribution. More specifically, while the meridional temperature gradient is much larger within the expanding than within the retreating cell, the near-surface temperature curvature is stronger within the retreating cell close to the ITCZ. These results seem to be consistent with arguments linking boundary layer convergence driven by SST gradients to the development of shallow circulations (e.g., Back & Bretherton, 2009). To the extent it drives the asymmetry in the seasonal evolution of the winter Hadley cell, the asymmetry in the near-surface temperature seasonal distribution appears to be crucial to the existence of a lag between the EFE and the ITCZ.

That the GMS cannot always be assumed as constant and that its changes need to be accounted for to understand the response of tropical precipitation to radiative perturbations have been highlighted by a few recent studies (e.g., Feldl & Bordoni, 2016; Merlis et al., 2013; Seo et al., 2017). In particular, Seo et al. (2017) show how changes in GMS dominate over changes in mass fluxes in the annual mean ITCZ response to doubling CO_2 in aquaplanet simulations with full-physics GCMs. Because of the GMS changes, the induced ITCZ shifts in those simulations are not explained by shifts in the EFE. Ours is the first study to show that this can also hold true when considering ITCZ migrations through the course of the seasonal cycle. Importantly, we show that the GMS can in fact become negative, which makes it possible for the EFE and the ITCZ to reside in oppo-

site hemispheres. Unfortunately, what determines the GMS remains an outstanding question (e.g., Raymond et al., 2009). Being dependent on both the vertical MSE distribution and the vertical structure of the large-scale circulation, the GMS depends on complex interactions between large-scale motions, convection, and clouds and has been shown to be very sensitive to different parameterizations (e.g., Seo et al., 2017). Negative values of GMS are, however, not an artifact of the simplified physics used in our idealized GCM, as they are also seen in seasonally varying aquaplanet simulations with comprehensive GCMs in the tropical rain belts with an annual cycle and a continent model intercomparison project (TRACMIP) archive (Voigt et al., 2016; Biasutti, personal communication, June 29, 2017). Future work leveraging the TRACMIP archive will explore the sensitivity of our results to the parameterized physics.

Overall, our results point to limitations of the atmospheric energy transport to provide quantitative predictions of ITCZ shifts on subseasonal time scales, with significant offsets in both amplitude and phase between the seasonal evolution of the EFE and that of the ITCZ. Across all simulations and at all times during the seasonal cycle, the best predictor of the ITCZ location is the maximum near-surface MSE, as expected from convective quasi-equilibrium views of tropical circulations. Given that the MSE distribution is itself influenced by the circulation, this association is, however, only diagnostic and itself falls short of a predictive theory. It is also important to emphasize how in our simulations tropical precipitation does not appear to be just controlled by thermodynamic constraints through local temperature (or MSE) maxima. In the Aqua0.2m simulation, and to some extent in the Aqua10m simulation, a secondary near-equatorial precipitation maximum exists in the summer hemisphere, whose location is more directly constrained by the curvature in the near-surface temperature distribution and, hence, by the boundary layer momentum budget (e.g., Lindzen & Nigam, 1987; Pauluis, 2004). The dynamics of this secondary ITCZ will be discussed elsewhere.

Some caveats are worth mentioning. Our results are based on simulations that are idealized both in terms of the zonally symmetric configuration and the represented physics. It is well known, for instance, that cloud feedbacks play an important role in the quantitative response of the tropical precipitation to a given radiative perturbation and that they are the major source of intermodel spread (e.g., Kang et al., 2008, 2009; Seo et al., 2017). Additionally, in Aqua0.2m the lower boundary has a thermal inertia that is more representative of values over land than ocean surfaces, allowing excursions of the convergence zones into subtropical latitudes similar to what is seen in Earth's monsoon regions (e.g., Bordoni & Schneider, 2008). Yet it differs from land in other important features, such as albedo and limited evaporation, which have nonnegligible effects on the energetics. The relevance of the mechanisms discussed here to monsoonal circulations as well as oceanic regions remains unclear. Analyses of observational data, both in the zonal mean and over oceanic and monsoon sectors, might shed some light on these open questions and will be pursued in future work. Vertical ascending motions that import MSE and have negative GMS are indeed observed over the East Pacific, where shallow circulations exist (e.g., Back & Bretherton, 2006; Zhang et al., 2004). These observed circulations and associated GMS should be reassessed within the atmospheric energy framework to explore their relationship with the ITCZ position and variability.

Finally, in our study we have neglected the possible role of ocean heat transport in seasonal ITCZ migrations. It is now well accepted that the mean northward position of the ITCZ primarily arises because the Atlantic Ocean transports energy from the southern to the NH (e.g., Frierson et al., 2013; Marshall et al., 2013). Moreover, theoretical arguments and modeling studies using fully coupled models show that changes in ocean heat transport can dampen the ITCZ response to energetic perturbations (e.g., Green & Marshall, 2017; Hawcroft et al., 2016; Schneider, 2017). Through its impact on SST distributions and cross-equatorial heat transport, ocean dynamics might therefore modify the mechanisms discussed in this study in important ways. An assessment of the impact of seasonally varying ocean heat transport in different basins on seasonal ITCZ shifts deserves further investigation.

Acknowledgments
This work was supported by the National Science Foundation (AGS-1462544). The numerical simulations and analyses were conducted on the Caltech's Division of Geological and Planetary Sciences CITerra high performance computing cluster. We thank Ori Adam, Larissa Back, David Battisti, Tobias Bischoff, Tim Cronin, Aaron Donohole, Spencer Hill, and Tapio Schneider for helpful discussion. The idealized GCM and all simulations are available at https://doi.org/10.22002/D1.933.

References

Adam, O., Bischoff, T., & Schneider, T. (2016a). Seasonal and interannual variations of the energy flux equator and ITCZ. Part I: Zonally averaged ITCZ position. *Journal of Climate*, *29*(9), 3219–3230. https://doi.org/10.1175/JCLI-D-15-0512.1

Adam, O., Bischoff, T., & Schneider, T. (2016b). Seasonal and interannual variations of the energy flux equator and ITCZ. Part II: Zonally varying shifts of the ITCZ. *Journal of Climate*, *29*(20), 7281–7293. https://doi.org/10.1175/JCLI-D-15-0710.1

Adler, R. F., Huffman, G. J., Chang, A., Ferraro, R., Xie, P.-P., Janowiak, J., et al. (2003). The version-2 Global Precipitation Climatology Project (GPCP) monthly precipitation analysis (1979–present). *Journal of Hydrometeorology*, *4*(6), 1147–1167. https://doi.org/10.1175/1525-7541(2003)004<1147:TVGPCP>2.0.CO;2

Arbuszewski, J. A., deMenocal, P. B., Cléroux, C., Bradtmiller, L., & Mix, A. (2013). Meridional shifts of the Atlantic intertropical convergence zone since the Last Glacial Maximum. *Nature Geoscience*, *6*(11), 959–962. https://doi.org/10.1016/j.epsl.2011.04.038

Back, L. E., & Bretherton, C. S. (2006). Geographic variability in the export of moist static energy and vertical motion profiles in the tropical Pacific. *Geophysical Research Letters*, *33*, L17810. https://doi.org/10.1029/2006GL026672

Back, L. E., & Bretherton, C. S. (2009). A simple model of climatological rainfall and vertical motion patterns over the tropical oceans. *Journal of Climate*, *22*(23), 6477–6497. https://doi.org/10.1175/2009JCLI2393.1

Bischoff, T., & Schneider, T. (2014). Energetic constraints on the position of the intertropical convergence zone. *Journal of Climate*, *27*(13), 4937–4951. https://doi.org/10.1175/JCLI-D-13-00650.1

Bordoni, S., & Schneider, T. (2008). Monsoons as eddy-mediated regime transitions of the tropical overturning circulation. *Nature Geoscience*, *1*(8), 515–519. https://doi.org/10.1038/ngeo248

Broccoli, A. J., Dahl, K. A., & Stouffer, R. J. (2006). Response of the ITCZ to Northern Hemisphere cooling. *Geophysical Research Letters*, *33*, L01702. https://doi.org/10.1029/2005GL024546

Chiang, J. C. H., Biasutti, M., & Battisti, D. S. (2003). Sensitivity of the Atlantic Intertropical Convergence Zone to Last Glacial Maximum boundary conditions. *Paleoceanography*, *18*(4), 1094. https://doi.org/10.1029/2003PA000916

Chiang, J. C. H., & Friedman, A. R. (2012). Extratropical cooling, interhemispheric thermal gradients, and tropical climate change. *Annual Review of Earth and Planetary Sciences*, *40*(1), 383–412. https://doi.org/10.1146/annurev-earth-042711-105545

Cronin, T. W., & Emanuel, K. A. (2013). The climate time scale in the approach to radiative-convective equilibrium. *Journal of Advances in Modeling Earth Systems*, *5*, 843–849. https://doi.org/10.1002/jame.20049

Donohoe, A., Marshall, J., Ferreira, D., & Mcgee, D. (2013). The relationship between ITCZ location and cross-equatorial atmospheric heat transport: From the seasonal cycle to the last glacial maximum. *Journal of Climate*, *26*(11), 3597–3618. https://doi.org/10.1175/JCLI-D-12-00467.1

Dwyer, J. G., Biasutti, M., & Sobel, A. H. (2012). Projected changes in the seasonal cycle of surface temperature. *Journal of Climate*, *25*(18), 6359–6374. https://doi.org/10.1175/JCLI-D-11-00741.1

Emanuel, K. A. (1995). On thermally direct circulations in moist atmospheres. *Journal of the Atmospheric Sciences*, *52*(9), 1529–1534. https://doi.org/10.1175/1520-0469(1995)052<1529:OTDCIM>2.0.CO;2

Faulk, S., Mitchell, J., & Bordoni, S. (2017). Effects of rotation rate and seasonal forcing on the ITCZ extent in planetary atmospheres. *Journal of the Atmospheric Sciences*, *74*(3), 665–678. https://doi.org/10.1175/JAS-D-16-0014.1

Feldl, N., & Bordoni, S. (2016). Characterizing the Hadley circulation response through regional climate feedbacks. *Journal of Climate*, *29*(2), 613–622. https://doi.org/10.1175/JCLI-D-15-0424.1

Feldl, N., Bordoni, S., & Merlis, T. M. (2017). Coupled high-latitude climate feedbacks and their impact on atmospheric heat transport. *Journal of Climate*, *30*(1), 189–201. https://doi.org/10.1175/JCLI-D-16-0324.1

Frierson, D. M. W. (2007). The dynamics of idealized convection schemes and their effect on the zonally averaged tropical circulation. *Journal of the Atmospheric Sciences*, *64*(6), 1959–1976. https://doi.org/10.1175/JAS3935.1

Frierson, D. M. W., Held, I. M., & Zurita-Gotor, P. (2006). A gray-radiation aquaplanet moist GCM. Part I: Static stability and eddy scale. *Journal of the Atmospheric Sciences*, *63*(10), 2548–2566. https://doi.org/10.1175/JAS3753.1

Frierson, D. M. W., Held, I. M., & Zurita-Gotor, P. (2007). A gray-radiation aquaplanet moist GCM. Part II: energy transports in altered climates. *Journal of the Atmospheric Sciences*, *64*(5), 1680–1693. https://doi.org/10.1175/JAS3913.1

Frierson, D. M. W., & Hwang, Y.-T. (2012). Extratropical influence on ITCZ shifts in slab ocean simulations of global warming. *Journal of Climate*, *25*(2), 720–733. https://doi.org/10.1175/JCLI-D-11-00116.1

Frierson, D. M. W., Hwang, Y.-T., Fučkar, N. S., Seager, R., Kang, S. M., Donohoe, A., et al. (2013). Contribution of ocean overturning circulation to tropical rainfall peak in the Northern Hemisphere. *Nature Geoscience*, *6*(10), 1–5. https://doi.org/10.1038/ngeo1987

Green, B., & Marshall, J. (2017). Coupling of trade winds with ocean circulation damps ITCZ shifts. *Journal of Climate*, *30*(12), 4395–4411. https://doi.org/10.1175/JCLI-D-16-0818.1

Haug, G. H. (2001). Southward migration of the intertropical convergence zone through the holocene. *Science*, *293*(5533), 1304–1308. https://doi.org/10.1126/science.1059725

Hawcroft, M., Haywood, J. M., Collins, M., Jones, A., Jones, A. C., & Stephens, G. (2016). Southern Ocean albedo, inter-hemispheric energy transports and the double ITCZ: Global impacts of biases in a coupled model. *Climate Dynamics*, *48*(7-8), 2279–2295. https://doi.org/10.1007/s00382-016-3205-5

Hill, S. A., Ming, Y., & Held, I. M. (2015). Mechanisms of forced tropical meridional energy flux change. *Journal of Climate*, *28*(5), 1725–1742. https://doi.org/10.1175/JCLI-D-14-00165.1

Hwang, Y.-T., Frierson, D. M. W., & Kang, S. M. (2013). Anthropogenic sulfate aerosol and the southward shift of tropical precipitation in the late 20th century. *Geophysical Research Letters*, *40*, 2845–2850. https://doi.org/10.1002/grl.50502

Kang, S. M., Frierson, D. M. W., & Held, I. M. (2009). The tropical response to extratropical thermal forcing in an idealized GCM: The importance of radiative feedbacks and convective parameterization. *Journal of the Atmospheric Sciences*, *66*(9), 2812–2827. https://doi.org/10.1175/2009JAS2924.1

Kang, S. M., Held, I. M., Frierson, D. M. W., & Zhao, M. (2008). The response of the ITCZ to extratropical thermal forcing: Idealized slab-ocean experiments with a GCM. *Journal of Climate*, *21*(14), 3521–3532. https://doi.org/10.1175/2007JCLI2146.1

Kaspi, Y., & Schneider, T. (2013). The role of stationary eddies in shaping midlatitude storm tracks. *Journal of the Atmospheric Sciences*, *70*(8), 2596–2613. https://doi.org/10.1175/JAS-D-12-082.1

Lea, D. W. (2003). Synchroneity of tropical and high-latitude atlantic temperatures over the last glacial termination. *Science*, *301*(5638), 1361–1364. https://doi.org/10.1126/science.1088470

Lin, J.-L. (2007). The double-ITCZ problem in IPCC AR4 coupled GCMS: Ocean–atmosphere feedback analysis. *Journal of Climate*, *20*(18), 4497–4525. https://doi.org/10.1175/JCLI4272.1

Lindzen, R. S., & Hou, A. V. (1988). Hadley circulations for zonally averaged heating centered off the equator. *Journal of the Atmospheric Sciences*, *45*(17), 2416–2427.

Lindzen, R. S., & Nigam, S. (1987). On the role of sea surface temperature gradients in forcing low-level winds and convergence in the tropics. *Journal of the Atmospheric Sciences*, *44*(17), 2418–2436. https://doi.org/10.1175/1520-0469(1987)044<2418:OTROSS>2.0.CO;2

Marshall, J., Donohoe, A., Ferreira, D., & McGee, D. (2013). The ocean's role in setting the mean position of the Inter-Tropical Convergence Zone. *Climate Dynamics*, *42*(7-8), 1967–1979. https://doi.org/10.1007/s00382-013-1767-z

Mcgee, D., Donohoe, A., Marshall, J., & Ferreira, D. (2014). Changes in ITCZ location and cross-equatorial heat transport at the Last Glacial Maximum, Heinrich Stadial 1, and the mid-Holocene. *Earth and Planetary Science Letters*, *390*, 69–79. https://doi.org/10.1016/j.epsl.2013.12.043

Merlis, T. M., Schneider, T., Bordoni, S., & Eisenman, I. (2013). The tropical precipitation response to orbital precession. *Journal of Climate*, *26*(6), 2010–2021. https://doi.org/10.1175/JCLI-D-12-00186.1

O'Gorman, P. A., & Schneider, T. (2008). The hydrological cycle over a wide range of climates simulated with an idealized GCM. *Journal of Climate*, *21*, 3815–3832. https://doi.org/10.1175/2007JCLI2065.1

Pauluis, O. (2004). Boundary layer dynamics and cross-equatorial Hadley circulation. *Journal of the Atmospheric Sciences*, *61*(10), 1161–1173.

Philander, S. G. H., Gu, D., Lambert, G., Li, T., Halpern, D., Lau, N. C., & Pacanowski, R. C. (1996). Why the ITCZ is mostly north of the equator. *Journal of Climate*, *9*(12), 2958–2972. https://doi.org/10.1175/1520-0442(1996)009<2958:WTIIMN>2.0.CO;2

Privé, N. C., & Plumb, R. A. (2007). Monsoon dynamics with interactive forcing. Part I: Axisymmetric studies. *Journal of the Atmospheric Sciences*, *64*(5), 1417–1430. https://doi.org/10.1175/JAS3916.1

Raymond, D. J., Sessions, S. L., Sobel, A. H., & Fuchs, Ž. (2009). the mechanics of gross moist stability. *Journal of Advances in Modeling Earth Systems*, *1*, 9. https://doi.org/10.3894/JAMES.2009.1.9

Schneider, T. (2017). Feedback of atmosphere-ocean coupling on shifts of the intertropical convergence zone. *Geophysical Research Letters*, *44*, 11,644–11,653. https://doi.org/10.1002/2017GL075817

Schneider, T., & Bordoni, S. (2008). Eddy-mediated regime transitions in the seasonal cycle of a Hadley circulation and implications for monsoon dynamics. *Journal of the Atmospheric Sciences*, *65*(3), 915–934. https://doi.org/10.1175/2007JAS2415.1

Seo, J., Kang, S. M., & Merlis, T. M. (2017). A model intercomparison of the tropical precipitation response to a CO_2 doubling in aquaplanet simulations. *Geophysical Research Letters*, *44*, 993–1000. https://doi.org/10.1002/2016GL072347

Singh, M. S., Kuang, Z., & Tian, Y. (2017). Eddy influences on the strength of the Hadley circulation: Dynamic and thermodynamic perspectives. *Journal of the Atmospheric Sciences*, *74*(2), 467–486. https://doi.org/10.1175/JAS-D-16-0238.1

Sobel, A. H. (2007). *The global circulation of the atmosphere* (pp. 219–251). Princeton, NJ: Princeton University Press.

Takahashi, K., & Battisti, D. S. (2007). Processes controlling the mean tropical Pacific precipitation pattern. Part I: The Andes and the Eastern Pacific ITCZ. *Journal of Climate*, *20*(14), 3434–3451. https://doi.org/10.1175/JCLI4198.1

Vellinga, M., & Wood, R. A. (2002). Global climatic impacts of a collapse of the Atlantic thermohaline circulation. *Climatic Change*, *54*(3), 251–267. https://doi.org/10.1023/A:1016168827653

Voigt, A., Biasutti, M., Scheff, J., Bader, J., Bordoni, S., Codron, F., et al. (2016). The tropical rain belts with an annual cycle and a continent model intercomparison project: TRACMIP. *Journal of Advances in Modeling Earth Systems*, *8*, 1868–1891. https://doi.org/10.1002/2016MS000748

Waliser, D. E., & Gautier, C. (1993). A satellite-derived climatology of the ITCZ. *Journal of Climate*, *6*(11), 2162–2174. https://doi.org/10.1175/1520-0442(1993)006<2162:ASDCOT>2.0.CO;2

Walker, C. C., & Schneider, T. (2005). Response of idealized Hadley circulations to seasonally varying heating. *Geophysical Research Letters*, *32*, L06813. https://doi.org/10.1029/2004GL022304

Walker, C. C., & Schneider, T. (2006). Eddy influences on Hadley circulations: Simulations with an idealized GCM. *Journal of the Atmospheric Sciences*, *63*(12), 3333–3350. https://doi.org/10.1175/JAS3821.1

Yoshimori, M., & Broccoli, A. J. (2008). Equilibrium response of an atmosphere–mixed layer ocean model to different radiative forcing agents: Global and zonal mean Response. *Journal of Climate*, *21*(17), 4399–4423. https://doi.org/10.1175/2008JCLI2172.1

Zhang, C. (2001). Double ITCZs. *Journal of Geophysical Research*, *106*(D11), 11,785–11,792. https://doi.org/10.1029/2001JD900046

Zhang, R., & Delworth, T. L. (2005). Simulated tropical response to a substantial weakening of the Atlantic thermohaline circulation. *Journal of Climate*, *18*(12), 1853–1860. https://doi.org/10.1175/JCLI3460.1

Zhang, C., McGauley, M., & Bond, N. A. (2004). Shallow meridional circulation in the tropical eastern Pacific. *Journal of Climate*, *17*(1), 133–139. https://doi.org/10.1175/1520-0442(2004)017<0133:SMCITT>2.0.CO;2